Instability in stratified accretion flows under primary and secondary perturbations

S. Nasraoui,[1] A. Salhi,[1] and T. Lehner[2]
[1]*Département de Physique, Faculté des Sciences de Tunis, 1060 Tunis, Tunisia*
[2]*LUTH, UMR 8102 CNRS, Observatoire de Paris-Meudon, 5 place de Janssen, F-92195 Meudon, France*
(Received 27 August 2014; revised manuscript received 23 February 2015; published 9 April 2015)

We consider horizontal linear shear flow (shear rate denoted by Λ) under vertical uniform rotation (ambient rotation rate denoted by Ω_0) and vertical stratification (buoyancy frequency denoted by N) in unbounded domain. We show that, under a primary vertical velocity perturbation and a radial density perturbation consisting of a one-dimensional standing wave with frequency N and amplitude proportional to $w_0 \sin(\varepsilon N x/w_0) \approx \varepsilon N x (\ll 1)$, where x denotes the radial coordinate and ε a small parameter, a parametric instability can develop in the flow, provided $N^2 > 8\Omega_0(2\Omega_0 - \Lambda)$. For astrophysical accretion flows and under the shearing sheet approximation, this implies $N^2 > 8\Omega_0^2(2-q)$, where $q = \Lambda/\Omega_0$ is the local shear gradient. In the case of a stratified constant angular momentum disk, $q = 2$, there is a parametric instability with the maximal growth rate $(\sigma_m/\varepsilon) = 3\sqrt{3}/16$ for any positive value of the buoyancy frequency N. In contrast, for a stratified Keplerian disk, $q = 1.5$, the parametric instability appears only for $N > 2\Omega_0$ with a maximal growth rate that depends on the ratio Ω_0/N and approaches $(3\sqrt{3}/16)\varepsilon$ for large values of N.

DOI: 10.1103/PhysRevE.91.043006 PACS number(s): 47.20.Cq, 47.27.Cn, 97.10.Gz

I. INTRODUCTION

The combination of horizontal plane shear, rotation, and vertical density stratification characterizes the dynamics of several astrophysical flows (e.g., cold accretion disks [1]) and geophysical flows (e.g., zonal geostrophic shear flows [2] and interaction of internal gravity waves with horizontally oceanic currents [3]). In the present paper, we consider stratified unbounded horizontal linear shear flow (shear rate denoted by Λ) in a frame rotating uniformly (ambient rotation rate denoted by Ω_0) about the vertical axis,

$$\boldsymbol{U} = -\Lambda x \boldsymbol{e}_y, \quad \overline{b} = N^2 z, \quad \boldsymbol{\Omega}_0 = \Omega_0 \boldsymbol{e}_z, \tag{1}$$

where $\overline{b}$ is the basic buoyancy scalar related to the basic density ϱ as $\overline{b} = -(g/\varrho_0)(\varrho - \varrho_0)$ and ϱ_0 is a reference density and g is the vertical gravity component. The vertical Brunt-Väisälä frequency, N, such that $N^2 = (\partial\overline{b}/\partial z)$, is assumed to be constant. Here (x,y,z) denotes the Cartesian coordinates system. We will show that the flow (1) can develop parametric instability under primary and secondary perturbations.

The simple flow (1) allows one to include the shearing sheet (or box) approximation (e.g., see Ref. [4]) used by many authors to study local instabilities in accretion disks such as the magnetorotational instability (MRI [5], see also the recent studies in Refs. [6,7]). For the accretion flows, the shear rate Λ is related to the rotation rate as $\Lambda = q\Omega_0$, where q is the local shear gradient and $\omega = \sqrt{2(2-q)}\ \Omega_0$ is the epicyclic frequency. For a Keplerian disk $q = 3/2$, $\omega = \Omega_0$ and for a constant angular momentum disk $q = 2$, $\omega = 0$. Otherwise, the rotation and shear rates can be independent as for geophysical flows.

As noticed by Goodman [8], the shearing sheet approximation contains most of the physics that is relevant to phenomena occurring on scales of order the disk thickness, H, or smaller. The essence of this approximation is local in approach, that is, the equations are valid in a small region (a Cartesian box) about a typical point in the disk. In the shearing sheet approximation, a steady flow consisting of a linear shear velocity profile in a frame rotating about the vertical axis solves the equations and one can consider it as a basic flow and perturb around it [9].

We consider that the Cartesian coordinates system (x,y,z) is centered at a reference point $P_0 = (r_0,\phi_0,0)$ in the midplane of the disk, rotating with the disk at angular velocity $\Omega_0 = \Omega(r_0)$ such that $x \equiv (r - r_0)$ is in the radial direction, $y \equiv r_0(\phi - \phi_0)$ is in the azimuthal direction, and $z \equiv z$ is in the axial direction. Thermally induced convection is included using the Boussinesq approximation (see, e.g., Refs. [9–11]). In this context, the equations for the perturbations around the base flow (1) are referred to as the shearing sheet approximation equations that can be written as follows in the inviscid limit (e.g., see Ref. [10]),

$$\begin{aligned}(\partial_t - \Lambda x\partial_y)\boldsymbol{u} + \boldsymbol{u}\cdot\boldsymbol{\nabla}\boldsymbol{u} &= -\boldsymbol{\nabla} p - 2\Omega_0 \boldsymbol{e}_z \times \boldsymbol{u} + \Lambda u \boldsymbol{e}_y + b\boldsymbol{e}_z,\\ (\partial_t - \Lambda x\partial_y)b + \boldsymbol{u}\cdot\boldsymbol{\nabla} b &= -N^2 w,\end{aligned} \tag{2}$$

with the incompressibility constraint, $\boldsymbol{\nabla}\cdot\boldsymbol{u} = 0$, where $\boldsymbol{u} = u\boldsymbol{e}_x + v\boldsymbol{e}_y + w\boldsymbol{e}_z$ is the velocity perturbation, b is the buoyancy scalar perturbation, and p denotes the pressure perturbation divided by the reference density ϱ_0. The third term $(\Lambda u \boldsymbol{e}_y)$ in the right-hand side of the first equation in system (2) characterizes the interaction between the perturbation velocity and the background shear. It generates the energy production term, $[\Lambda\langle uv\rangle]$, in the equation for the kinetic energy $E_c = (1/2)\langle u^2 + v^2 + w^2\rangle$, where $\langle\cdot\rangle$ denotes an average over space. As for the term $(-N^2 w)$ in the right-hand side of the second equation in system (2), it characterizes the interaction between the perturbation velocity and the background buoyancy scalar. It generates the vertical buoyancy flux $[-\langle wb\rangle]$ in the equation for the potential energy $E_p = (1/2)N^{-2}\langle b^2\rangle$. Because the equation for E_c involves the term $[\langle wb\rangle]$, the buoyancy flux does not contribute to net energetics, but it is responsible for energy exchange between the kinetic and the potential forms (e.g., see Ref. [3]).

Linear stability analysis of system (2) under plane-wave disturbances with time-dependent wave vector $\boldsymbol{k}(t) = (k_{10} +$

 ©2015 American Physical Society

$k_2\Lambda t, k_2, k_3)$, where $\boldsymbol{k}_0 = (k_{10}, k_2, k_3)$ is the initial wave vector (at $t = 0$), has been addressed in several works (e.g., see Ref. [12]). These advected plane-wave disturbances (e.g., see Ref. [13]) are often called spatial Fourier harmonics (SFH) [14] and sometimes Kelvin modes (e.g., from Ref. [15]). When $2\Omega_0\,(2\Omega_0 - \Lambda) > 0$ and $N^2 > 0$, the solution is bounded as $Nt \to \infty$. In fact, under axisymmetric disturbances (i.e., $k_2 = 0$, so $\boldsymbol{k}$ is time independent) the solution exhibits an oscillatory behavior with frequency ω_p such that [see also the first equation in system (35)]

$$\omega_p^2 = \frac{k_3^2}{k_{10}^2 + k_3^2}\omega^2 + \frac{k_{10}^2}{k_{10}^2 + k_3^2}N^2. \tag{3}$$

On other words, there are rotating-sheared-gravity waves propagating in the (x_1, x_3) plane with frequency ω_p. Under nonsymmetric perturbations (i.e., $k_2 \neq 0$, so $\boldsymbol{k}$ is time-dependent) the solutions of system (2) are asymptotically bounded converging toward an oscillating wave state at frequency N (see Salhi *et al.* [12]). In counterpart, the time evolution of total energy (kinetic+potential) can exhibit important transient growth (see Sec. IVC). This is a consequence of the non-normality of the linear operators governing perturbation in these linear shear flows (see, e.g., Ref. [16]). Energy transition growth in linear shear flows has been proposed as a mechanism that generates turbulence to support accretion process in cold accretion disks (see, e.g., Refs. [12,17–19]). Note that Mukhopadhyay [20] showed that three-dimensional secondary perturbation to the primary perturbed (nonstratified) disk, consisting of elliptical vortices, gives significantly large hydrodynamic growth and then possible nonlinear feedback and turbulence in accretion flows. Recently, Marcus *et al.* [1], who studied the dynamics and formation of vortices in flow (1), found that the vortices self-similarity (i.e., zombie vortices) replicate to create lattices of turbulent vortices, which suggests that they may have an important role in star and planet formation. For geophysical flows, Bakas and Farrell [3], who investigated the interaction of internal gravity waves with (nonrotating) unbounded horizontal shear flow, found that the two mechanisms that are, respectively, due to advection of zonal velocity and to downgradient Reynolds stresses produce large and robust amplification of zonal velocity and/or density and vertical velocity, potentially leading to shear or convective instability.

In the present paper, we show that, under axisymmetric secondary disturbances, a parametric instability can occur in flow (1). For instance, in the case of a stratified Keplerian disk the parametric instability can occurs only for $\mathrm{Ri} = N^2/(q^2\Omega_0^2) > 16/9$. When $\mathrm{Ri} < 16/9$, we briefly examine the behavior of the spectral density of energy considering asymmetric disturbances ($k_2 \neq 0$) in order to see whether the primary perturbation enhances the transient growth. The paper is organized as follows. Section II deals with the mathematical formulation. For axisymmetric disturbances, the stability problem, which is governed by a Floquet system, is presented in Sec. III. Computations and some analytical results are presented in Sec. IV. Transient growth of energy for asymmetric disturbances is briefly addressed in Sec. IV. Our concluding remarks are presented in Sec. V.

II. PRIMARY AND SECONDARY PERTURBATIONS

A. Primary perturbation

We consider a primary perturbation that depends only on the radial coordinate and on the time,

$$\boldsymbol{u} = w(x,t)\boldsymbol{e}_z, \quad b = b(x,t), \quad p = p(x,t). \tag{4}$$

Substituting the above form into Eq. (2), which is reported here for the sake of clarity,

$$\begin{aligned}
&(\partial_t - \Lambda x\partial_y)u + \boldsymbol{u}\cdot\nabla u = -\partial_x p + 2\Omega_0 v,\\
&(\partial_t - \Lambda x\partial_y)v + \boldsymbol{u}\cdot\nabla v = -\partial_y p - 2\Omega_0 u + \Lambda u,\\
&(\partial_t - \Lambda x\partial_y)w + \boldsymbol{u}\cdot\nabla w = -\partial_z p + b,\\
&(\partial_t - \Lambda x\partial_y)b + \boldsymbol{u}\cdot\nabla b = -N^2 w,
\end{aligned} \tag{5}$$

we obtain

$$\begin{aligned}
&\partial_t w = b, \quad \partial_t b = -N^2 w,\\
&\nabla p = 0, \quad \partial_{tt}^2 w(x,t) + N^2 w(x,t) = 0.
\end{aligned} \tag{6}$$

An exact solution of the latter differential equations is of the form

$$w(x,t) = h(x)\sin(Nt), \quad b = Nh(x)\cos(Nt), \quad p = 0,$$

where $h(x)$ represents any function of the radial coordinate. In a similar manner to the background velocity which varies linearly with the radial coordinate, we consider a primary perturbation for which $h(x)$ varies linearly with the radial coordinate:

$$\begin{aligned}
&\boldsymbol{u}_p = w(x,t)\boldsymbol{e}_z = \varepsilon Nx\sin(Nt)\boldsymbol{e}_z,\\
&b_p = b(w,x) = \varepsilon N^2 x\cos(Nt),
\end{aligned} \tag{7}$$

with $p_b = 0$, where ε is a small parameter since

$$\begin{aligned}
&\frac{\|\boldsymbol{u}_p\|}{\|\boldsymbol{U}\|} = \frac{N\varepsilon|\sin(Nt)|}{\Lambda} \leqslant \frac{N\varepsilon}{\Lambda} \ll 1,\\
&\frac{|b_p|}{|\bar{b}|} = \frac{N^2\varepsilon|\cos(Nt)|}{N^2} \leqslant \varepsilon \ll 1.
\end{aligned} \tag{8}$$

Also, the following form for which $h(x)$ exhibits an oscillatory behavior is an exact solution of Eq. (5)

$$\begin{aligned}
&\boldsymbol{u}_p = w_0\sin\left(\frac{\varepsilon N}{w_0}x\right)\sin(Nt)\boldsymbol{e}_z,\\
&b_p = w_0 N\sin\left(\frac{\varepsilon N}{w_0}x\right)\cos(Nt),
\end{aligned} \tag{9}$$

with $p_b = 0$, where w_0 is a positive constant. The solution (9) characterizes a standing wave that results from the superposition of the two plane waves propagating along the opposite (radial) directions $\pm\boldsymbol{e}_x$. When

$$\varepsilon \ll \frac{w_0}{xN} \ll 1,$$

the solution (7) well approximates the solution (9). On other words, the solution (7) can be seen as a local approximation of a standing wave with frequency N and amplitude

$$\begin{aligned}
w_0\sin\left(\frac{\varepsilon Nx}{w_0}\right) &= w_0\sum_{n=0}^{\infty}(-1)^n\frac{(\varepsilon Nx/w_0)^{(2n+1)}}{(2n+1)!}\\
&= \varepsilon Nx + \ldots.
\end{aligned}$$

Recall that both the forms (7) and (9) are exact solutions of the system in Eq. (6) [or Eq. (5)].

B. Secondary perturbation

In addition to the primary perturbation we consider further perturbation (secondary one) $(\boldsymbol{u}',p',b')$ such as

$$\begin{aligned} \boldsymbol{u} &= \boldsymbol{u}' + xN\varepsilon\sin\tau\,\boldsymbol{e}_z, \\ p &= p', \\ b &= b' + xN^2\varepsilon\cos\tau, \end{aligned} \tag{10}$$

where $\tau = Nt$ is a dimensionless time in which N has an arbitrary positive value. Substituting the form (10) into system (5) and using the following developments:

$$\begin{aligned} (\boldsymbol{u}\cdot\boldsymbol{\nabla})\boldsymbol{u} &= (\boldsymbol{u}'\cdot\boldsymbol{\nabla})\boldsymbol{u}' + (xN\varepsilon\sin\tau)\partial_z\boldsymbol{u}' + (N\varepsilon\sin\tau)u'\boldsymbol{e}_z, \\ (\boldsymbol{u}\cdot\boldsymbol{\nabla})b &= (\boldsymbol{u}'\cdot\boldsymbol{\nabla})b' + (xN\varepsilon\sin\tau)\partial_z b' + (N^2\varepsilon\cos\tau)u', \end{aligned} \tag{11}$$

we obtain

$$\begin{aligned} \frac{Du'}{Dt} + \boldsymbol{u}'\cdot\boldsymbol{\nabla}u' &= -\partial_x p' + 2\Omega_0 v', \\ \frac{Dv'}{Dt} + \boldsymbol{u}'\cdot\boldsymbol{\nabla}v' &= -\partial_y p' - 2\Omega_0 u' + \Lambda u', \\ \frac{Dw'}{Dt} + \boldsymbol{u}'\cdot\boldsymbol{\nabla}w' &= -\partial_z p' - (N\varepsilon\sin\tau)\,u' + b', \\ \frac{Db'}{Dt} + \boldsymbol{u}'\cdot\boldsymbol{\nabla}b' &= -\left(N^2\varepsilon\cos\tau\right)u' - N^2 w', \end{aligned} \tag{12}$$

with the incompressibility constraint $\boldsymbol{\nabla}\cdot\boldsymbol{u}' = 0$. Here

$$\frac{D}{Dt}(\boldsymbol{u}',b') = [\partial_t - \Lambda x\partial_y + (N\varepsilon x\sin\tau)\partial_z](\boldsymbol{u}',b').$$

As stressed in the Introduction, the main purpose of the present study is to perform a linear stability analysis for the base flow (1) under primary and secondary perturbations. Therefore, we begin by linearizing the system (12), i.e., we neglect the nonlinear terms $(\boldsymbol{u}'\cdot\boldsymbol{\nabla})\boldsymbol{u}'$ and $(\boldsymbol{u}'\cdot\boldsymbol{\nabla})b'$. Accordingly, the resulting linearized system reads

$$\begin{aligned} \frac{Du'}{Dt} &= -\partial_x p' + 2\Omega_0 v', \\ \frac{Dv'}{Dt} &= -\partial_y p' - 2\Omega_0 u' + \Lambda u', \\ \frac{Dw'}{Dt} &= -\partial_z p' - (N\varepsilon\sin\tau)u' + b', \\ \frac{Db'}{Dt} &= -(N^2\varepsilon\cos\tau)u' - N^2 w' \end{aligned} \tag{13}$$

with the incompressibility constraint $\boldsymbol{\nabla}\cdot\boldsymbol{u}' = 0$. The system (13) can be seen as the linearized system for a perturbation superimposed to the basic flow $(\boldsymbol{U} + \boldsymbol{u}_p) = \mathbf{A}\cdot\boldsymbol{x}$, where

$$A_{ij} = -\Lambda\delta_{i2}\delta_{j1} + (N\varepsilon\sin\tau)\delta_{i3}\delta_{j1}, \tag{14}$$

and $(\bar{b} + b_p) = N^2(z + x\varepsilon\cos\tau)$. Note that the case where there is no horizontal shear (i.e., $\Lambda = 0$) has been addressed by Ref. [21].

As will be shown later, the potential vorticity (PV)

$$\varpi = [\boldsymbol{\nabla}\times(\boldsymbol{U} + \boldsymbol{u}_p + \boldsymbol{u}') + 2\boldsymbol{\Omega}_0]\cdot[\boldsymbol{\nabla}(\bar{b} + b_p + b')],$$

which is a Lagrangian invariant for an inviscid and nondiffusive fluid, is relevant for a stability analysis of system (13). Therefore, we report here its linear part,

$$\begin{aligned} \varpi' = (2\Omega_0 - \Lambda)\partial_z b' - N\varepsilon\sin\tau\,\partial_y b' + N^2(\partial_x v' - \partial_y u') \\ + N^2\varepsilon\cos\tau(\partial_y w' - \partial_z v'). \end{aligned} \tag{15}$$

The background PV, $\overline{\varpi} = N^2\Omega_0(2-q)$, is positive for $0 \leqslant q < 2$ and vanishes for a constant angular momentum disk, $q = 2$.

C. Plane-wave disturbances

It is known that, an unbounded, uniformly rotating flow supports a spectrum of inertial oscillations consisting of traveling waves whose wave vectors rotate with the flow. Viewed from the inertial frame, these modes may be written as

$$(\boldsymbol{u}', N^{-1}p', N^{-1}b') = (\hat{\boldsymbol{u}},\hat{p},\hat{b})\exp[\mathrm{i}\boldsymbol{k}(t)\cdot\boldsymbol{x}]. \tag{16}$$

a form of sufficient generality to describe oscillations upon any flow with spatially uniform strain rates (e.g., see Refs. [13,22–26]). These advected plane-wave disturbances (e.g., see Ref. [13]) are often called spatial Fourier harmonics (SFH) [14], as indicated in the Introduction. Substituting the form (16) into (13), we have

$$\begin{aligned} \dot{\hat{\boldsymbol{u}}} + \mathrm{i}[(\dot{\boldsymbol{k}} + N^{-1}\mathbf{A}^T\cdot\boldsymbol{k})\cdot\boldsymbol{x}]\hat{\boldsymbol{u}} &= -\mathrm{i}\hat{p}\boldsymbol{k} - 2\Omega_0^*\boldsymbol{e}_z\times\hat{\boldsymbol{u}} + \hat{b}\boldsymbol{e}_z \\ &\quad + (q\Omega_0^*\boldsymbol{e}_y - \varepsilon\sin\tau\,\boldsymbol{e}_z)\hat{u} \\ \dot{\hat{b}} + \mathrm{i}[(\dot{\boldsymbol{k}} + N^{-1}\mathbf{A}^T\cdot\boldsymbol{k})\cdot\boldsymbol{x}]\hat{b} &= -(\varepsilon\cos\tau)\hat{u} - \hat{w}, \end{aligned} \tag{17}$$

where $\dot{\boldsymbol{u}} = d\boldsymbol{u}/d\tau$ is the derivative with respect to the dimensionless time $\tau = Nt$, the exponent T denotes the transpose, and $\Omega_0^* = \Omega_0/N$. The term proportional to $\boldsymbol{x}$ must vanish since the above equations must be valid for any $\|\boldsymbol{x}\|$. This is ensured when (see, e.g., Ref. [13])

$$\dot{\boldsymbol{k}} = -N^{-1}\mathbf{A}^T\cdot\boldsymbol{k}. \tag{18}$$

Using the form of A_{ij} given by Eq. (14), we obtain

$$\begin{aligned} k_1(\tau) &= k_{10} + q\Omega_0^* k_2\tau - \varepsilon k_3(1-\cos\tau), \\ k_2 &= k_2, \\ k_3 &= k_3, \end{aligned} \tag{19}$$

where $\boldsymbol{k}_0 = (k_{10},k_2,k_3)$ is the initial wave vector (at $t = 0$). Only the radial component of the wave vector is time dependent, while the vertical and azimuthal components, k_2 and k_3, remain unaffected by shear. Hereafter, we denote by $k_\perp = \sqrt{k_2^2 + k_3^2}$, which is time independent, and by $k = \|\boldsymbol{k}\|$ the modulus of the wave vector $\boldsymbol{k}$ where

$$\dot{k} = k^{-1}k_1\dot{k}_1 = q\Omega_0^* k^{-1}k_1 k_2 - \varepsilon k^{-1}k_1 k_3\sin\tau. \tag{20}$$

By using both the incompressibility constraint, $\boldsymbol{k}\cdot\hat{\boldsymbol{u}} = 0$, and Eq. (18), we derive from the first equation in system (17) the expression of the pressure mode $\hat{p}$,

$$-\mathrm{i}k^2\hat{p} = [2(1-q)\Omega_0^* k_2 + 2(\varepsilon\sin\tau)k_3]\hat{u} - 2\Omega_0^* k_1\hat{v} - k_3\hat{b}. \tag{21}$$

Substituting the latter relation into system (17), we obtain

$$\begin{aligned}
\dot{\hat{u}} &= \left[2(1-q)\,\Omega_0^*\frac{k_1k_2}{k^2} + (2\varepsilon\sin\tau)\,\frac{k_1k_3}{k^2}\right]\hat{u} \\
&\quad +2\Omega_0^*\left(1-\frac{k_1^2}{k^2}\right)\hat{v} - \frac{k_1k_3}{k^2}\hat{b}, \\
\dot{\hat{v}} &= \left\{\Omega_0^*\left[(q-2)+2(1-q)\,\frac{k_2^2}{k^2}\right] + (2\varepsilon\sin\tau)\,\frac{k_2k_3}{k^2}\right\}\hat{u} \\
&\quad -2\Omega_0^*\frac{k_1k_2}{k^2}\hat{v} - \frac{k_2k_3}{k^2}\hat{b}, \\
\dot{\hat{w}} &= \left[(2-q)\,\Omega_0^*\frac{k_2k_3}{k^2} + (\varepsilon\sin\tau)\left(2\frac{k_3^2}{k^2}-1\right)\right]\hat{u} \\
&\quad -2\Omega_0^*\frac{k_1k_3}{k^2}\hat{v} + \left(1-\frac{k_3^2}{k^2}\right)\hat{b} \\
\dot{\hat{b}} &= -(\varepsilon\cos\tau)\,\hat{u} - \hat{w},
\end{aligned} \tag{22}$$

while the spectral counterpart of the linear part of PV given by Eq. (15) takes the form

$$\begin{aligned}
\hat{\pi} &= -\mathrm{i}\hat{\varpi}/N^2 = [\Omega_0^*(2-q)k_3 - k_2\varepsilon\sin\tau]\hat{b} - k_2\hat{u} \\
&\quad + (k_{10} - \varepsilon k_3 + q\Omega_0^*k_2\tau)\hat{v} + (k_2\varepsilon\cos\tau)\hat{w}.
\end{aligned} \tag{23}$$

Recall that PV is a Lagrangian invariant for an inviscid and nondiffusive fluid, i.e., $\hat{\pi} = \text{const}$.

III. FLOQUET SYSTEM FOR AXISYMMETRIC DISTURBANCES

In this section, we consider axisymmetric disturbances, i.e., those corresponding to a zero value for the azimuthal wave number. In that case, the system (22) reduces to a Floquet system. We will show that the stability of that Floquet system is governed by the behavior of the trace of the Floquet fundamental matrix solution $\mathbf{g}$.

For axisymmetric disturbances (i.e., $k_2 = 0$), the wave vector becomes time periodic,

$$k_1(\tau) = k_{10} - \varepsilon k_3\,(1-\cos\tau), \quad k_2 = 0, \quad k_3 = k_3,$$

with period 2π. In the following, we consider that $k_3 \neq 0$ since, at $k_2 = k_3 = 0$, the system (17) yields

$$\hat{u} = 0, \quad \hat{v} = \hat{v}_0, \quad \dot{\hat{w}} = \hat{b}, \quad \ddot{\hat{b}} + \hat{b} = 0,$$

indicating stability (i.e., the solution is bounded as $\tau \to \infty$). Therefore, at $k_2 = 0$ and $k_3 \neq 0$, the system (17) reduces to

$$\begin{aligned}
\dot{\hat{u}} &= 2(\varepsilon\sin\tau)\,\frac{k_1k_3}{k^2}\hat{u} + 2\Omega_0^*\frac{k_3^2}{k^2}\hat{v} - \frac{k_1k_3}{k^2}\hat{b}, \\
\dot{\hat{v}} &= (q-2)\,\Omega_0^*\hat{u}, \\
\dot{\hat{b}} &= \frac{(k_{10}-\varepsilon k_3)}{k_3}\hat{u},
\end{aligned} \tag{24}$$

with $\hat{w} = -(k_1/k_3)\hat{u}$. Moreover, because the potential vorticity counterpart $\hat{\pi}$ is time independent, it is more convenient for the stability analysis to consider the differential system for the following three variables:

$$\begin{aligned}
\hat{c}_1 &= \frac{1}{k_0}\hat{\pi} = (2-q)\,\Omega_0^*\frac{k_3}{k_0}\hat{b} + \frac{(k_{10}-\varepsilon k_3)}{k_0}\hat{v}, \\
\hat{c}_2 &= \frac{k^2}{k_0^2}\frac{(k_{10}-\varepsilon k_3)}{k_0}\hat{u}, \quad \hat{c}_3 = \hat{b},
\end{aligned} \tag{25}$$

instead of the differential system for $(\hat{u},\hat{v},\hat{b})$, where $k_0 = \sqrt{k_{10}^2 + k_3^2}$. Therefore, the Floquet system for $\hat{\boldsymbol{c}} = (\hat{c}_1,\hat{c}_2,\hat{c}_3)$ is equivalent to the following vector equation:

$$\dot{\hat{\boldsymbol{c}}} = \mathbf{D}\cdot\hat{\boldsymbol{c}}, \tag{26}$$

where the nonzero elements of the matrix $\mathbf{D}$ are

$$\begin{aligned}
D_{21} &= 2\Omega_0^*\frac{k_3^2}{k_0^2}, \\
D_{23} &= -\omega^{*2}\frac{k_3^3}{k_0^3} - \frac{(k_{10}-\varepsilon k_3)\,k_1k_3}{k_0^3}, \\
D_{32} &= \frac{k_0^3}{k_3k^2},
\end{aligned} \tag{27}$$

in which $\omega^* = \omega/N$. Though not always analytically solvable, the temporal behavior of $\hat{\boldsymbol{c}}$ may be characterized by using the standard Floquet theory since the matrix $\mathbf{D}(\tau)$ is time periodic with period 2π. The general solution is a linear combination of three modes $\exp(\sigma_i\tau)\,f_i(\tau)\,(i = 1,2,3)$, where $f_i(\tau)$ is periodic with period 2π (see, e.g., Refs. [22,27]). The Floquet exponent σ_i is determined by the requirement that $\exp(2\pi\sigma_i)$ is an eigenvalue (or the Floquet multiplier) of the Floquet matrix $\mathbf{g}(2\pi)$, where $\mathbf{g}(\tau)$ is the fundamental matrix solution of system (26), i.e.,

$$\dot{\mathbf{g}} = \mathbf{D}\cdot\mathbf{g} \tag{28}$$

with $g_{ij}(0) = \delta_{ij}$. Its eigenvalues, say, λ_1, λ_2, and λ_3, are the roots of the algebraic equation

$$-\lambda^3 + (\mathrm{tr}\,\mathbf{g})\,\lambda^2 - \mathrm{II}_g\lambda + (\det\mathbf{g}) = 0, \tag{29}$$

where the invariants $(\mathrm{tr}\,\mathbf{g}) = g_{jj}$ and $(\det\mathbf{g})$ are, respectively, the trace and the determinant of the matrix $\mathbf{g}$, and

$$\mathrm{II}_g = g_{11}g_{22} + g_{11}g_{33} + g_{22}g_{33} - g_{12}g_{21} - g_{13}g_{31} - g_{23}g_{32}.$$

Because $(\mathrm{tr}\,\mathbf{D}) = 0$, the determinant of $\mathbf{g}$ is unity, $(\det\mathbf{g}) = 1$. This property provides a ready check on the accuracy of the numerical procedure used to calculate $\mathbf{g}$ (see Sec. IIIB). In addition, the fact that the potential vorticity counterpart is a constant, i.e., $\dot{\hat{c}}_1 = 0$, implies that

$$g_{11} = 1, \quad g_{12} = g_{13} = 0,$$

and, hence,

$$\begin{aligned}
&\det\mathbf{g} = g_{22}g_{33} - g_{23}g_{32} = 1, \\
&\mathrm{II}_g = (1 + g_{22} + g_{33}) + (g_{22}g_{33} - g_{23}g_{32} - 1) = \mathrm{tr}\,\mathbf{g}.
\end{aligned} \tag{30}$$

Accordingly, one easily deduces from (29) that one eigenvalue is unity, say, $\lambda_1 = 1$, and

$$\lambda_2 = \frac{1}{2}[(\mathrm{tr}\,\mathbf{g} - 1) + \sqrt{(\mathrm{tr}\,\mathbf{g} - 1)^2 - 4}], \quad \lambda_3 = \frac{1}{\lambda_2}. \tag{31}$$

There is instability whenever

$$\mathrm{Re}\sigma_i > 0, \quad \sigma_i = \frac{1}{2\pi}\log\lambda_i$$

with $i = 2$ or $i = 3$.

In the light of the latter analysis, we may conclude that one can only consider the reduced Floquet system for the elements g_{22}, g_{23}, g_{32}, and g_{33}, i.e.,

$$\dot{g}_{2i} = D_{23}g_{3i}, \quad \dot{g}_{3i} = D_{32}g_{2i} \tag{32}$$

($i = 2,3$), for which there is instability whenever $|g_{22} + g_{33}| > 2$. Moreover, an alternative formulation of system (32) as a single second-order equation yields

$$\frac{d}{d\tau}\left(D_{32}^{-1}\frac{dg_{3i}}{d\tau}\right) = D_{23}g_{3i},$$

or, equivalently,

$$\frac{d^2}{d\tau^2}\left(\frac{k}{k_0}g_{3i}\right) + \left[\frac{\omega^2}{N^2}\frac{k_3^2}{k^2} + \frac{k_1^2}{k^2} - \varepsilon^2\frac{k_3^4}{k^4}\sin^2\tau\right]\left(\frac{k}{k_0}g_{3i}\right) = 0. \tag{33}$$

Since the coefficients are periodic in τ, this has the form of a Hill's equation (see Ref. [28]). As will be shown in the next section, at sufficiently small ε, some analytical results can be found by applying perturbation techniques to the Hill's equation (33).

IV. RESULTS AND DISCUSSION

Computations were used to determine the time evolution of (tr **g**) at $\tau = 2\pi$. A fourth-order Runge-Kutta scheme with time step $\delta\tau = 10^{-4}\pi$ has been used to perform the numerical integration of the system (32) for $q = \Lambda/\Omega_0 = 2$ (a constant angular-momentum disk) and $q = 3/2$ (a Keplerian disk) and several values of the Richardson number, $\mathrm{Ri} = N^2/(q^2\Omega_0^2)$. Because, at sufficiently small ε, there is an expected agreement between the numerical results and analytical results obtained by applying perturbation techniques (see [29]) to the Hill's equation (33), we first present these analytical results.

A. Some analytical results

1. *The resonant points of the $\varepsilon = 0$ axis*

We seek an expansion for the solution $\Psi(\tau) = (k/k_0)g_{3i}$ of (33) and also for the coefficients that depend on ε in power series of ε in the form

$$\begin{aligned} k_1^2(\tau) &= k_0^2\left[\frac{k_{10}^2}{k_0^2} - 2\varepsilon\frac{k_{10}k_3}{k_0^2}(1-\cos\tau) + \ldots\right], \\ k^{-2}(\tau) &= k_0^{-2}\left[1 + 2\varepsilon\frac{k_{10}k_3}{k_0^2}(1-\cos\tau) + \ldots\right], \\ \Psi(\tau) &= \frac{k(\tau)}{k_0}g_{3i}(\tau) = \Psi_0(\tau) + \varepsilon\Psi_1(\tau) + \ldots. \end{aligned} \tag{34}$$

In the following, we limit ourselves to $\mathcal{O}(\varepsilon)$. Accordingly, substituting (34) into (33) and equating coefficients of equal powers of ε, we have

$$\begin{aligned} &\frac{d^2\Psi_0}{d\tau^{*2}} + 4\omega_p^{*2}\Psi_0 = 0, \\ &\frac{d^2\Psi_1}{d\tau^{*2}} + 4\omega_p^{*2}\Psi_1 = -2\beta_0(\cos(2\tau^*) - 1)\Psi_0, \end{aligned} \tag{35}$$

where $\tau^* = \tau/2$,

$$\beta_0 = 4\frac{k_{10}k_3^3}{k_0^4}(1-\omega^{*2}), \tag{36}$$

$\omega_p^* = \omega_p/N$ and $\omega^* = \omega/N$. Recall that $\omega_p^2 = (\omega^2k_3^2 + N^2k_{10}^2)/k_0^2$ is the frequency of the rotating-sheared-gravity waves propagating in the (x_1,x_3) plane (see Sec. I), and ω is the epicyclic frequency. The solution of the first equation in (35) is of the form $\Psi_0(\tau^*) = a_0\cos(2\omega_p^*\tau^* + \phi_0)$, where a_0 and ϕ_0 are constants. Disregarding the homogeneous solution of the second equation in (35), the solution $\Psi_1(\tau^*)$ is found as

$$\begin{aligned} \Psi_1 = &\frac{a_0\beta_0}{4}\frac{\cos[2(\omega_p^*+1)\tau^* + \phi_0]}{(1+2\omega_p^*)} \\ &+ \frac{a_0\beta_0}{4}\frac{\cos[2(\omega_p^*-1)\tau^* + \phi_0]}{(1-2\omega_p^*)}. \end{aligned} \tag{37}$$

Due to the presence of small divisor terms, the above expansion breaks down when

$$\omega_{p\,|\varepsilon=0}^* = \left[\omega^{*2}\frac{k_3^2}{k_0^2} + \frac{k_{10}^2}{k_0^2}\right]^{\frac{1}{2}} = \pm\frac{1}{2}, \tag{38}$$

and, hence,

$$\mu_{|\varepsilon=0} = \cos\alpha = \frac{k_{10}}{k_0} = \pm\frac{1}{2}\left[\frac{q^2\mathrm{Ri} + 8q - 16}{q^2\mathrm{Ri} + 2q - 4}\right]^{\frac{1}{2}}, \tag{39}$$

where $0 \leqslant \alpha \leqslant \pi$ since Eq. (33) is invariant under the interchange $\alpha \to \alpha + \pi$. In the $(\varepsilon,\alpha = \cos^{-1}\mu)$ plane, the points of the $\varepsilon = 0$ axis from which emanate the unstable regions, if reachable, are characterized by Eq. (39).

2. *The curves separating the stable and unstable regions*

To characterize the transition curves between stable and unstable regions we expand $4\omega_p^{*2}$ around unity in powers of ε (called the method of strained parameters, see Eq. [29]) in addition to the expansions given by Eq. (34),

$$4\omega_p^{*2} = 1 + \varepsilon\delta_1 + \ldots. \tag{40}$$

Substituting Eqs. (34) and (40) into the Eq. (33) gives

$$\begin{aligned} &\frac{d^2\Psi_0}{d\tau^{*2}} + \Psi_0 = 0, \\ &\frac{d^2\Psi_1}{d\tau^{*2}} + \Psi_1 = -\delta_1\Psi_0 - 2\beta_0[\cos(2\tau^*) - 1]\Psi_0. \end{aligned} \tag{41}$$

The general solution of the first equation in (41) is

$$\Psi_0 = a_1\cos\tau^* + a_2\sin\tau^*, \tag{42}$$

where a_1 and a_2 are constants. Substituting the latter solution into the second equation in (41), we obtain

$$\begin{aligned} \frac{d^2\Psi_1}{d\tau^{*2}} + \Psi_1 = &a_1(\beta_0 - \delta_1)\cos\tau^* + a_2(3\beta_0 - \delta_1)\sin\tau^* \\ &-\beta_0[a_1\cos(3\tau^*) + a_2\sin(3\tau^*)]. \end{aligned} \tag{43}$$

Eliminating the terms that produce secular terms in Ψ_1 demands that $\delta_1 = \beta_0$ and $a_2 = 0$ or $\delta_1 = 3\beta_0$ and $a_1 = 0$. It follows that the equations characterizing the transition curves are of the form

$$4\omega_p^{*2} = 1 + \varepsilon\beta_0 \quad \text{or} \quad 4\omega_p^{*2} = 1 + 3\varepsilon\beta_0. \tag{44}$$

Therefore, in the $(\varepsilon,\alpha = \cos^{-1}\mu)$ plane, the transition curves at $\mathcal{O}(\varepsilon)$ are characterized by the following algebraic equations:

$$\begin{aligned} 4\mu^2 - 4\varepsilon\mu(1-\mu^2)^{\frac{3}{2}} - \left[\frac{q^2\mathrm{Ri} + 8q - 16}{q^2\mathrm{Ri} + 2q - 4}\right] = 0, \\ 4\mu^2 - 12\varepsilon\mu(1-\mu^2)^{\frac{3}{2}} - \left[\frac{q^2\mathrm{Ri} + 8q - 16}{q^2\mathrm{Ri} + 2q - 4}\right] = 0, \end{aligned} \tag{45}$$

for sufficiently small ε. For a given value of the triplet $(q,\mathrm{R}i,\varepsilon)$ we resolve the algebraic equation (45) by using the Newton's method and determine the μ value.

3. *The maximal growth rate of the instability*

To determine the maximal growth rate of the instabilities we use the normal or Floquet forms of the solutions (i.e., the Whittaker's method, see Ref. [29]), and put

$$\Psi(\tau^*) = \exp(\gamma\tau^*) f(\tau^*), \tag{46}$$

where $f(\tau^* + \pi) = f(\tau^*)$ according to Floquet theory, as indicated at the beginning of Sec. IIIA. Recall that $\tau^* = \tau/2$. Near the transition curves the exponent γ is small, and, hence, we seek an expansion in the form

$$\begin{aligned} f(\tau^*,\varepsilon) &= f_0(\tau^*) + \varepsilon f_1(\tau^*) + \ldots \\ 4\omega_p^{*2} &= 1 + \varepsilon\delta_1 + \ldots \\ \gamma &= \varepsilon\gamma_1 + \ldots, \end{aligned} \tag{47}$$

in addition to the two first expansions in Eq. (34). Substituting the form (47) and the two first equations in (34) into the Hill's equation (33), we obtain

$$\begin{aligned} &\frac{d^2 f_0}{d\tau^{*2}} + f_0 = 0, \\ &\frac{d^2 f_1}{d\tau^{*2}} + f_1 = -2\gamma_1 \frac{df_0}{d\tau^*} - \delta_1 f_0 - 2\beta_0(\cos(2\tau^*) - 1) f_0. \end{aligned} \tag{48}$$

Substituting the solution $f_0 = a_1\cos\tau^* + a_2\sin\tau^*$ into the second equation in (48) gives

$$\begin{aligned} \frac{d^2 f_1}{d\tau^{*2}} + f_1 = {} & [2\gamma_1 a_1 + (3\beta_0 - \delta_1) a_2]\sin\tau^* \\ & + [(\beta_0 - \delta_1) a_1 - 2\gamma_1 a_2]\cos\tau^* \\ & - \beta_0[a_1\cos(3\tau^*) + a_2\sin(3\tau^*)]. \end{aligned} \tag{49}$$

Eliminating the terms that produce secular terms in f_1, we have

$$\begin{aligned} 2\gamma_1 a_1 + (3\beta_0 - \delta_1) a_2 = 0 \\ (\beta_0 - \delta_1) a_1 - 2\gamma_1 a_2 = 0. \end{aligned} \tag{50}$$

A nontrivial solution of (50) requires that

$$4\gamma_1^2 - (3\beta_0 - \delta_1)(\delta_1 - \beta_0) = 0. \tag{51}$$

From the latter relation, it is clear that γ_1 vanishes when $\delta_1 = \beta_0$ or $\delta_1 = 3\beta_0$. Moreover, by setting $\delta_1 = a\beta_0$, one easily verifies that $\gamma_1(a)$ is maximal at $a = 2$, so $\delta_1 = 2\beta_0$, and, hence, $\gamma_m \equiv \varepsilon\gamma_1|_{a=2} = \varepsilon\beta_0/2$, or, equivalently, in the original variable $(\tau = 2\tau^*)$,

$$\sigma_m = \frac{1}{2}\gamma_m = \frac{3\sqrt{3}}{16}\frac{\left[1 - \frac{8(2-q)}{q^2\mathrm{Ri}}\right]^{\frac{1}{2}}}{\left[1 - \frac{2(2-q)}{q^2\mathrm{Ri}}\right]}\varepsilon \tag{52}$$

for sufficiently small ε. It should be noted that Whitaker's method, which yields a uniform approximation in the solutions of Eq. (33) on and near the transition curves, is valid only for linear problems as the one addressed here. For nonlinear problems, this method does not apply and the method of multiple scales can rather be used to treat such problems (e.g., see Refs. [27,29]).

B. Comparison with numerical results

Numerical results for a constant angular momentum disk, $q = 2$, are shown in Figs. 1(a)–1(d) obtained at $\mathrm{Ri} = 0.5$. In Figs. 1(a) and 1(b) the horizontal axis is ε and the vertical one is α/π such that $0 \leqslant \alpha \leqslant \pi$ since Eq. (33) is invariant under the interchange $\alpha \to \alpha + \pi$, as indicated previously. The plotted curves show two regions of instability that emanate from the points $(\varepsilon = 0,\alpha = \pi/3)$ and $(\varepsilon = 0,\alpha = 2\pi/3)$, respectively, in agreement with Eq. (39), which yields, at $q = 2,\alpha = \cos^{-1}(\pm 0.5)$, independently of the Ri value. The width of these two unstable regions is not the same: The width of the second region of instability (for which $k_{10}k_3 < 0$ or $\pi/2 < \alpha < \pi$) is larger than the one of the first region of instability (for which $k_1k_3 > 0$ or $0 < \alpha < \pi/2$). Also, the results yielded by Eq. (45) show that the width of the unstable region for which $\pi/2 < \alpha < \pi$ is larger than the width of the unstable region for which $0 < \alpha < \pi/2$, as illustrated in Fig. 1(d). As can be expected from Fig. 1(b), when $\varepsilon < 0.2$, the agreement is good between the numerical results and Eq. (45) that characterizes the (neutral) curves separating the stable and unstable regions, but this deteriorates as $\varepsilon(\geqslant 0.2)$ increases.

Figure 1(c) describes how the maximum growth rate varies with ε within the tongue. As can be seen, both the two regions of instability have the same maximum growth rate. The limit $\varepsilon \to 0$, corresponds to the scaled growth rate $\sigma_m/\varepsilon \approx 0.3247$. The latter numerical results is in agreement with the analytical one given by Eq. (52), $[\sigma_m/\varepsilon]_{q=2} = 3\sqrt{3}/16 \approx 0.3247$. Note that, in Fig. 1(a), the dashed lines indicate the inclination a of largest growth rate at a given ε.

Accordingly, we may conclude that for both the constant angular momentum accretion flow (i.e., $q = 2$) the primary perturbation generates a parametric instability for which the maximal growth rate does not depend on Ri.

Similar results were found for $0 < q < 2$ except the fact that instability is not attainable for any positive value of the Richardson number. In fact, according to both computations and the analytical results [see Eq. (39)], there is no instability emanating from the $\varepsilon = 0$ axis when $\mathrm{Ri} \leqslant 8(2-q)/q^2$. For a Keplerian disk, $q = 1.5$, the parametric instability emanating from the $\varepsilon = 0$ axis is then attainable only when $\mathrm{Ri} > 16/9 \approx 1.778$. Figures 2(a) and 2(b) show the parametric tongues of instability emerging from the axis $\varepsilon = 0$ for $(q = 1.5,$

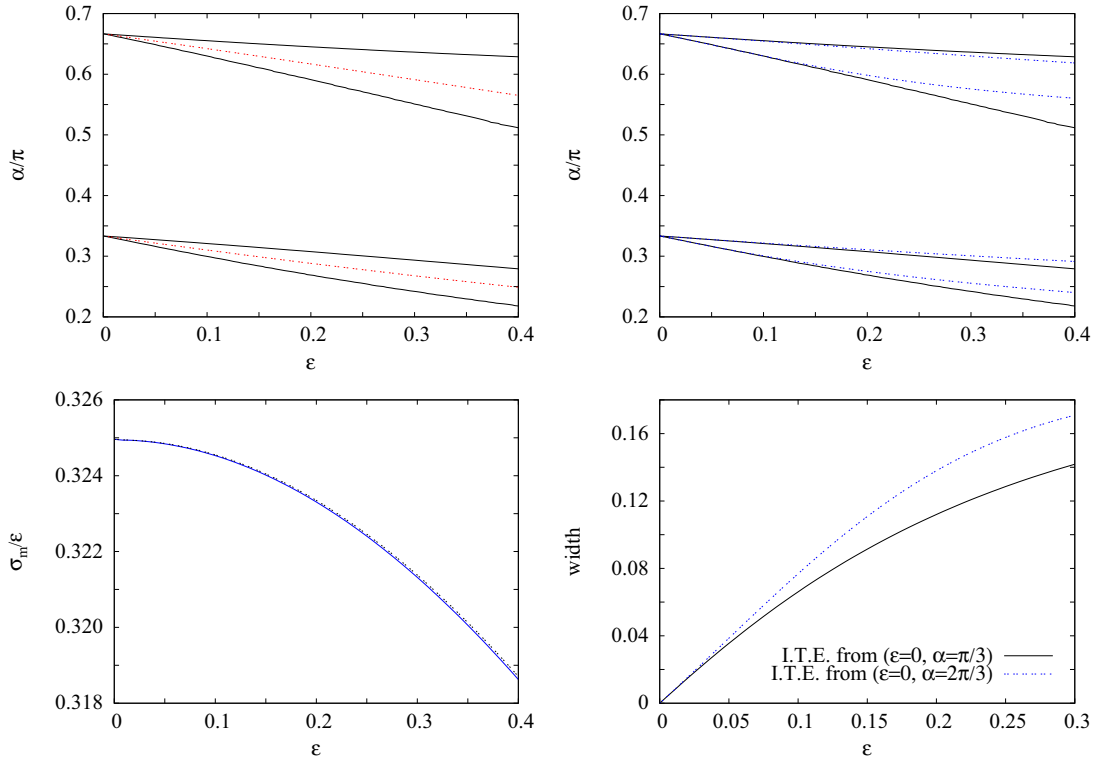

FIG. 1. (Color online) A stratified constant angular momentum disk, $q = 2$, under primary and secondary axisymmetric perturbations. Top left panel: The Floquet tongues of instability as a function of the parameter ε (numerical results). Within the subharmonic tongue emanating from $\alpha = \cos^{-1}(\pm 0.5)$, the dashed lines indicate the inclination a of largest growth rate (plotted in the bottom left panel) at a given ε. Top right panel: Comparison between computations and analytical results [see Eqs. (39) and (45)]. Bottom left panel: A plot of the maximum scaled growth rate against the parameter ε (numerical results). The intercept is $3\sqrt{3}/16$, in agreement with the analytical result [see Eq. (52)]. Bottom right panel: Width of the instability tongues emanating (I.T.E.) from $\alpha = \cos^{-1}(\pm 0.5)$ as a function of the parameter ε [analytical results from Eq. (45)].

$\mathrm{Ri} = 2.0$) and ($q = 1.5$,$\mathrm{Ri} = 3.0$), respectively. The agreement between the analytical results given by Eq. (45) and the numerical ones is good for $\varepsilon < 0.2$, but this deteriorates as $\varepsilon(\gtrsim 0.2)$ [see Fig. 2(d)]. At ($q = 1.5$,$\mathrm{Ri} = 2.0$), the unstable regions emanate from $\alpha = \cos^{-1}[\pm 1/(2\sqrt{7})] \approx 0.43948$ or 0.5605, while at ($q = 1.5$,$\mathrm{Ri} = 3.0$), they emanate from $\alpha = \cos^{-1}[\pm\sqrt{11}/(2\sqrt{23})] \approx 0.3876$ or 0.6124, in agreement with the analytical results yielded by Eq. (39). The variation of the maximum growth rate σ_m/ε against ε for $q = 1.5$ and $\mathrm{Ri} = 2.5$, 3.0, 10.0 is shown in Fig. 2(c). At $\varepsilon = 0$, the values of σ_m/ε yielded by computations corresponding to $\mathrm{Ri} = 2.5$, 3.0, and 10.0, are $3\sqrt{1755}/592 \approx 0.2122$,$3\sqrt{891}/368 \approx 0.2433$, and $9\sqrt{555}/688 \approx 0.3081$, respectively, in agreement with Eq. (52).

C. Transient growth of energy for asymmetric disturbances

For asymmetric disturbances, i.e., $k_2 \neq 0$, the wave vector is not periodic and the stability problem requires us to determine the behavior of the solution of system (22) as $\tau \to \infty$. This will be treated in a subsequent paper. In this section, we simply determine numerically the spectral density of energy in the case of a Keplerian disk and we analyze its behavior for particular orientations of the initial wave vector and $0 < \mathrm{Ri} < 16/9$, in connection to the results found in the case where $\varepsilon = 0$ addressed in the study by Ref. [12].

For the determination of the spectral density of energy, it is more convenient to consider the following modes:

$$u^{(1)} = \frac{k_3}{k_\perp}\hat{v} - \frac{k_2}{k_\perp}\hat{w}, \quad u^{(2)} = -\frac{k}{k_\perp}\hat{u}, \quad u^{(3)} = \hat{b}, \tag{53}$$

since the spectral density of kinetic energy $\mathcal{E}_c$ can simply expressed as

$$\mathcal{E}_c = \tfrac{1}{2}(\langle|u^{(1)}|^2\rangle + \langle|u^{(2)}|^2\rangle), \quad \mathcal{E}_p = \tfrac{1}{2}\langle|u^{(3)}|^2\rangle,$$

while $\mathcal{E}_p$ represents the spectral density of potential energy. Therefore, the differential system for these modes, which is equivalent to system (22), takes the form (see the appendix),

$$\begin{aligned}
\frac{d}{d\tau}u^{(1)} &= \left[\Omega_0^*(2-q)\frac{k_3}{k} - (\varepsilon\sin\tau)\frac{k_2}{k}\right]u^{(2)} - \frac{k_2}{k_\perp}u^{(3)} \\
\frac{d}{d\tau}(ku^{(2)}) &= -2\Omega_0^* k_3 u^{(1)} + k_1 k_3 k_\perp^{-1} u^{(3)} \\
\frac{d}{d\tau}u^{(3)} &= \frac{k_2}{k_\perp}u^{(1)} - \left(\frac{k_1 k_3}{k_\perp k} - \frac{k_\perp}{k}\varepsilon\cos\tau\right)u^{(2)}.
\end{aligned} \tag{54}$$

Let $\mathbf{G}$ be the fundamental matrix solution of system (54), i.e., $u^{(i)}(\tau) = G_{ij}u^{(j)}(0)$ $(i,j = 1,2,3)$. It is governed by the same equation as $(u^{(1)},u^{(2)},u^{(3)})$ is but with universal initial condition $G_{ij}(0) = \delta_{ij}$ $(i,j = 1,2,3)$. The fourth-order Runge-Kutta method with the step size $\delta\tau = 10^{-4}$ were used to integrate that system to determine the time evolution of G_{ij}

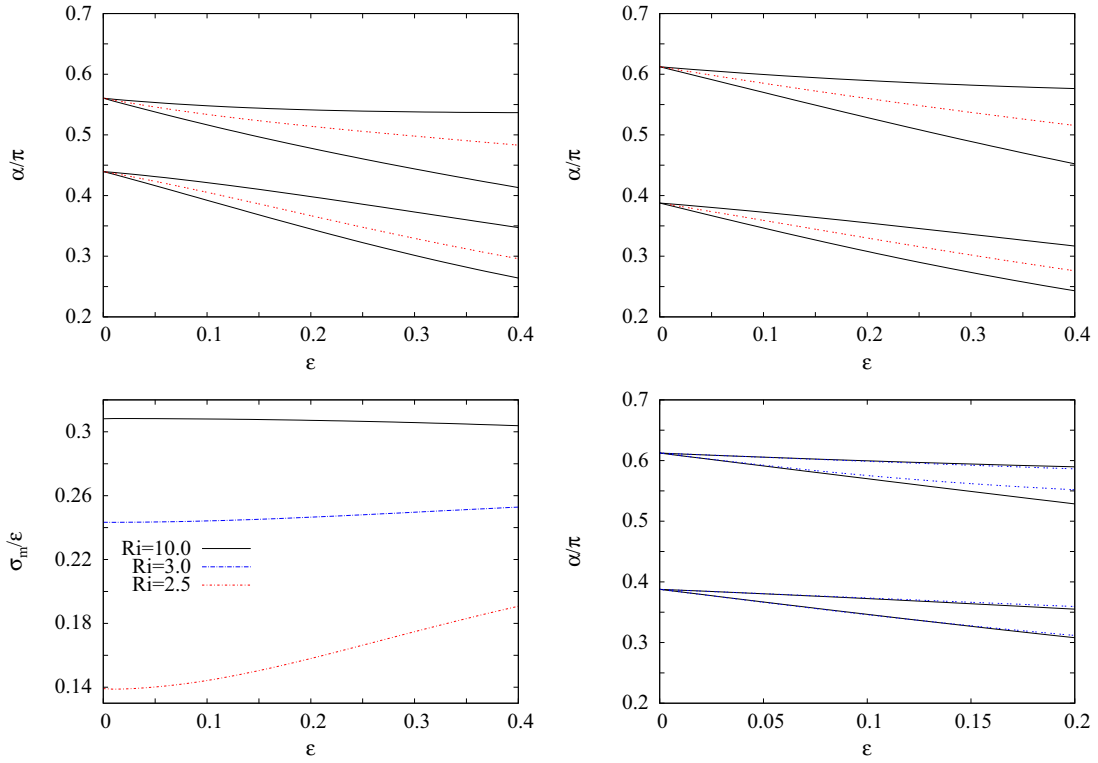

FIG. 2. (Color online) A stratified Keplerian disk, $q = 1.5$, under primary and secondary axisymmetric perturbations. Top panels: The Floquet tongues of instability as a function of the parameter ε (numerical results) for Ri = 2.0 (left panel) and Ri = 3.0 (right panel). Within the subharmonic tongue emanating from $\alpha = \cos^{-1}[\pm 0.5\sqrt{(9\mathrm{Ri}-16)/(9\mathrm{Ri}-4)}]$, the dashed lines indicate the inclination a of largest growth rate (plotted in the bottom left panel) at a given ε. Bottom left panel: A plot of the maximum scaled growth rate against the parameter ε (numerical results) for Ri = 2.5, 3.0, 10.0. The intercept is $(3\sqrt{3}/16)\sqrt{1-16/(9\mathrm{Ri})}/\,[(1-4/(9\mathrm{Ri})]$, in agreement with the analytical result [see Eq. (52)]. Bottom right panel: Comparison between computations and analytical results for Ri = 3.0 [see Eqs. (39) and (45)].

for given ε, q, Ri, and $\boldsymbol{k}(0)/k(0)$. Accuracy was easily assessed by evaluating the determinant of $\mathbf{G}$, $\det \mathbf{G} = k(0)/k(\tau)$.

Computations indicate that the elements G_{ij} exhibit an oscillatory behavior with period that is insensitive to the variation of ε, whereas the amplitude can be affected by the primary perturbation ($\varepsilon \neq 0$). This is illustrated by Fig. 1(a), which displays the time history of the element G_{11} for $q = 1.5$, Ri = 0.5, $k_{10}/k_2 = 100$, $k_3/k_{10} = 0.5$, and $\varepsilon = 0.0,\ 0.1,\ 0.2$. For the given ε and after the initial phase characterized by $0 \leqslant \tau < \tau_0$ such that $k_1(\tau_0) = 0$, the amplitude of oscillations becomes more important. During the initial phase, the variation of ε does not induce appreciable variations of the amplitude and the period of the oscillations, whereas after the initial phase, only the amplitude increases with an increasing of ε.

As indicated in Sec. I, although the base flow (1) is stable (i.e., there are no exponentially growing solutions, see Ref. [12]), it can exhibit significant transient growth in energy because of the nonnormality of perturbation dynamics due to shear. In the bypass transition to turbulence, which has been developed by the hydrodynamic community for spectrally stable shear flows, perturbations undergo a transient growth. If they have an initially finite amplitude, they may reach an amplitude that is sufficiently large to allow positive feedback through nonlinear interactions that repopulate the growing disturbances (e.g., see Ref. [16]. This mechanism could plausibly sustain turbulence for large-enough Reynolds numbers. This concept was adopted for unmagnetized stratified accretion disks, since there is irrefutable observational evidence that Keplerian disks have to be turbulent (e.g., see Ref. [19]).

For initial isotropic conditions with vanishing initial potential energy,

$$\begin{aligned} \mathcal{E}_c(0) &= \left\langle \left| u_0^{(1)} \right|^2 \right\rangle = \left\langle \left| u_0^{(2)} \right|^2 \right\rangle, \\ \mathcal{E}_p(0) &= \tfrac{1}{2}\left\langle \left| u_0^{(3)} \right|^2 \right\rangle = 0, \end{aligned} \tag{55}$$

we have computed the time evolution of the spectral density of total energy, $\mathcal{E} = \mathcal{E}_c + \mathcal{E}_p$, normalized by its initial value,

$$\gamma_E = \frac{\mathcal{E}(\tau)}{\mathcal{E}(0)} = \sum_{i=1}^{3}\sum_{j=1}^{2} |G_{ij}|^2. \tag{56}$$

Under the same conditions as in Fig. 1(a), Fig. 1(b) shows the time history γ_E. As can be expected, there is an important increase of γ_E during the initial phase. This phase can be called the transient growth phase. The physical mechanism of this growth is rather due to the background shear (e.g., see Ref. [30]). After this initial phase, γ_E approaches its long-time limit, which corresponds to an important level of energy. The primary perturbation acts to increase the level of energy as shown by Fig. 1(b) since, after the transient growth phase, γ_E increases as ε increases.

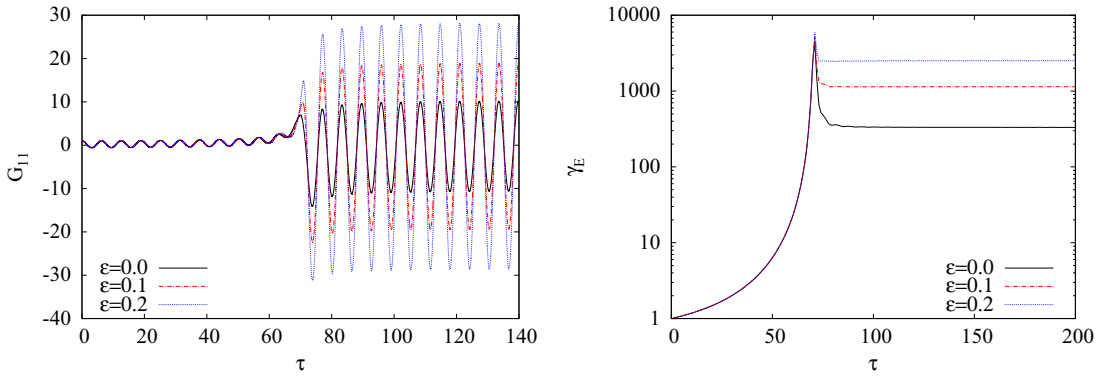

FIG. 3. (Color online) A stratified Keplerian disk, $q = 1.5$, under primary and secondary asymmetric perturbations, $k_{10}/k_2 = 100, k_3/k_2 = 0.5$. Left panel: Time evolution of the element G_{11} of the fundamental matrix solution of system (54) for Ri $= 0.5$ and $\varepsilon = 0.0, 0.1, 0.2$. Right panel: Time evolution of the spectral density of total (kinetic+potential) energy normalized by its initial value under initial isotropic conditions with vanishing initial potential energy for Ri $= 0.5$ and $\varepsilon = 0.0, 0.1, 0.2$.

A detailed analysis of the transient amplification of non-symmetric perturbations for Ri $> 16/9$ will be examined further in a subsequent paper to characterize the dynamic of the wave-vortex mode coupling and to see whether the transient growth rate of energy prevails over twice the maximal growth rate of the parametric instability (if attainable). In fact, for baroclinic sheared flows, it is found that asymmetric perturbations undergo substantial transient amplification much larger than the growth of symmetric instability (see Refs. [31,32]).

V. CONCLUDING REMARKS

In the present study, we have performed a linear stability analysis of horizontal linear shear under vertical uniform rotation and vertical stratification with a constant strength N^2 in unbounded domain [see Eq. (1)]. The dynamic of a perturbation around this basic state is governed by Eq. (2). That equation is the same as the one derived in the background of the shearing sheet approximation characterizing locally the flow dynamic in astrophysical accretion disks. Recall that the essence of this approximation is local in approach, that is, the equations are valid in a small region (a Cartesian box) about a typical point in the disk [9]. Both primary and secondary perturbations to the base flow described by Eq. (1) were considered. A primary perturbation consisting of a standing wave, with amplitude $w_0 \sin(\varepsilon N x/w_0)$, that results from a superposition of plane waves with frequency N propagating in the opposite radial directions, is an exact solution of Eq. (2). In accordance with the shearing sheet approximation, locally, the amplitude can be approximated by a linear variation with respect to the radial coordinate provided $\varepsilon \ll w_0/(xN) \ll 1$. This leads to the form (7), which is also an exact solution of equation of system (2). In the present study, the form (7) has been considered as a primary perturbation. A plane wave with an advected wave vector is considered for the secondary perturbation.

With the help of the potential vorticity, which is a constant of motion for an inviscid and nondiffusive fluid, it has been shown that the stability problem for the axisymmetric secondary disturbances reduces to a two-dimensional Floquet system [see Eq. (32)] or, equivalently, to a Hill's equation [see Eq. (33)]. For sufficiently small ε, we have applied a perturbation technique to the Hill's equation and derived some analytical results: The points lying on the $\varepsilon = 0$ axis from which emanate the instability regions [see Eq. (39)], the equations characterizing the curves separating stable and unstable regions [see Eq. (45)], and the maximal growth rate of the instability in the limit $\varepsilon \to 0$ [see Eq. (52)]. For two accretion flows, a constant angular momentum disk, $q = 2$, and a Keplerian disk, $q = 1.5$, the analytical results have been compared to computations. At $\varepsilon < 0.2$, the analytical results are in good agreement with the numerical ones but this deteriorates when $\varepsilon \geqslant 0.2$. It is found that the apparition of the parametric instability in a Keplerian disk requires a nonweak stratification [Ri $= N^2/(q^2\Omega_0^2) > 16/9$], such that the disk may not support it. In the case of a constant angular-momentum disk, the parametric instability occurs even for very weak stratification.

In the case of asymmetric disturbances ($k_2 \neq 0$), we have determined numerically the time evolution of the spectral density of energy, normalized by its initial value, for some particular values of the initial wave vector. With respect to the case where $\varepsilon = 0$, which is linearly stable (i.e., the solution is bounded as $\tau \to \infty$) as proved in the study by Ref. [12], it is found that, during the initial phase $0 \leqslant \tau < \tau_0$ such that $k_1(\tau_0) = 0$, the primary perturbation has no appreciable effect on the transient growth. After this initial period during which there is a gain of energy induced by the interaction between the perturbed field and the background shear, the important level of energy maintained beyond this phase for large times becomes more important in the presence of the primary perturbation [see Fig. 3(b)]. The stability of the base flow (1) under primary and asymmetric secondary perturbations, as well as the dynamic of the wave-vortex mode coupling in that flow, will be treated in detail in a subsequent paper.

ACKNOWLEDGMENTS

A. Salhi acknowledges the hospitality at the Laboratory PIIM, UMR 7345 CNRS (Aix-Marseille University) and at the Loboratory LUTH, UMR 8102 CNRS (Observatoire Paris-Meudon).

APPENDIX

Derivation of the differential system for the modes $(u^{(1)},u^{(2)},u^{(3)})$

Due to Eq. (18), the system (17) reduces to

$$\begin{aligned}\dot{\hat{u}} &= -ik_1\hat{p} + 2\Omega_0^*\hat{v},\\ \dot{\hat{v}} &= -ik_2\hat{p} - \Omega_0^*(2-q)\hat{u},\\ \dot{\hat{w}} &= -ik_3\hat{p} - (\varepsilon\sin\tau)\,\hat{u} + \hat{b},\\ \dot{\hat{b}} &= -(\varepsilon\cos\tau)\,\hat{u} - \hat{w},\end{aligned} \tag{A1}$$

with the incompressibility constraint $\boldsymbol{k}\cdot\hat{\boldsymbol{u}} = 0$. We multiply the second equation with k_3 and the third equation with $(-k_2)$. Then we add the resulting equations to obtain

$$k_3\hat{v} - k_2\hat{w} = -[\Omega_0^*(2-q)k_3 - (\varepsilon\sin\tau)k_2]\hat{u} - k_2\hat{b}. \tag{A2}$$

On the other hand, we multiply the second equation in system (A1) by k_2 and the third equation by k_3. Then we add the resulting equations and obtain

$$\begin{aligned}-ik_\perp^2\hat{p} &= -\frac{d}{d\tau}(k_1\hat{u}) + [(2-q)\,\Omega_0^*k_2 + (\varepsilon\sin\tau)\,k_3]\hat{u} - k_3\hat{b}\\ &= -k_1\dot{\hat{u}} - 2(\dot{k}_1 - \Omega_0^*k_2)\hat{u} - k_3\hat{b}.\end{aligned} \tag{A3}$$

Recall that $k\dot{k} = k_1\dot{k}_1$, where $\dot{k}_1 = q\Omega_0^*k_2 - (\varepsilon\sin\tau)k_3$, and $k_\perp = \sqrt{k_2^2+k_3^2}$, which is time independent.

Substituting Eq. (A3) into the first equation in system (A1), we obtain

$$\frac{d}{d\tau}(k^2\hat{u}) = 2\Omega_0^*k_1k_2\hat{u} + 2\Omega_0^*k_\perp^2\,\hat{v} - k_1k_3\hat{b}. \tag{A4}$$

By introducing the three modes $(u^{(1)},u^{(2)},u^{(3)})$ such that

$$u^{(1)} = \frac{k_3}{k_\perp}\hat{v} - \frac{k_2}{k_\perp}\hat{w}, \quad u^{(2)} = -\frac{k}{k_\perp}\hat{u} \tag{A5}$$

and $u^{(3)} = \hat{b}$ or, equivalently,

$$\hat{v} = \frac{k_3}{k_\perp}u^{(1)} + \frac{k_1k_2}{k_\perp k}u^{(2)}, \quad \hat{w} = -\frac{k_2}{k_\perp}u^{(1)} + \frac{k_1k_3}{k_\perp k}u^{(2)} \tag{A6}$$

with $\hat{u} = (-k_\perp/k)u^{(2)}$ and $\hat{b} = u^{(3)}$, we transform Eqs. (A2) and (A4) and the fourth equation in system (A1) in terms of the three modes $(u^{(1)},u^{(2)},u^{(3)})$, and, hence, we recover system (54).

[1] P. S. Marcus, S. Pei, C. H. Jiang, and P. Hassanzadeh, Phys. Rev. Lett. **111**, 084501 (2013).
[2] M. V. Kalashnick, G. R. Mamatsashvili, G. D. Chagelishvili, and J. G. Lominadze, Q. J. R. Meteorol. Soc. **132**, 505 (2006).
[3] N. A. Bakas and B. F. Farrel, J. Phys. Oceanogr. **39**, 497 (2009).
[4] P. Goldreich and D. Lynden-Bell, Mon. Not. R. Astron. Soc. **130**, 125 (1965).
[5] S. A. Balbus and J. F. Hawley, Astrophys. J. **376**, 214 (1991).
[6] A. Salhi, T. Lehner, F. Godeferd, and C. Cambon, Phys. Rev. E **85**, 026301 (2012).
[7] J. Squire and A. Bhattacharjee, Phys. Rev. Lett. **113**, 025006 (2014).
[8] J. Goodman, Astrophys. J. **406**, 596 (1993).
[9] O. M. Umurhan and O. Regev, Astron. Astrophys. **427**, 855 (2004).
[10] O. M. Umurhan, Mon. Not. R. Astron. Soc. Lett. **365**, 85 (2006).
[11] G. Lesur and I. Ogilvie, Mon. Not. R. Astron. Soc. Lett. **404**, L64 (2010).
[12] A. Salhi, T. Lehner, F. S. Godeferd, and C. Cambon, Astrophys. J. **771**, 103 (2013).
[13] A. D. D. Craik and W. O. Criminale, Proc. R. Soc. Lond. A **406**, 13 (1986).
[14] G. D. Chagelishvili, A. G. Tevzadze, G. Bodo, and S. S. Moiseev, Phys. Rev. Lett. **79**, 3178 (1997).
[15] H. K. Moffatt, in *Atmospheric Turbulence and Radio Wave Propagation* (Nauka, Moscow, 1967), pp. 139–156.
[16] P. J. Schmid and D. S. Henningson, *Stability and Transition in Shear Flows* (Springer, Berlin, 2001).
[17] P. A. Yecko, Astron. Astrophys. **425**, 385 (2004).
[18] B. Mukhopadhyay, N. Afshordi, and R. Narayan, Astrophys. J. **629**, 383 (2005).
[19] A. G. Tevzadze, G. D. Chagelishvili, and J. P. Zahn, Astron. Astrophys. **478**, 9 (2008).
[20] B. Mukhopadhyay, Astrophys. J. **653**, 503 (2006).
[21] A. Salhi and S. Nasraoui, Phys. Rev. E **88**, 063016 (2013).
[22] B. J. Bayly, Phys. Rev. Lett. **57**, 2160 (1986).
[23] A. D. D. Craik, J. Fluid Mech. **198**, 275 (1989).
[24] A. D. D. Craik and H. R. Allen, J. Fluid Mech. **234**, 613 (1992).
[25] R. R. Kerswell, Annu. Rev. Fluid Mech. **34**, 83 (2002).
[26] A. Salhi and C. Cambon, Phys. Rev. E **81**, 026302 (2010).
[27] P. Glendinning, *Stability, Instability and Chaos* (Cambridge University Press, Cambridge, UK, 1994).
[28] S. Magnus and W. Winkler, *Hills Equation* (John Wiley & Sons, New York, 1966).
[29] A. H. Nayfeh, *Introduction to Perturbation Techniques* (John Wiley & Sons, New York, 1981).
[30] A. Salhi and A. B. Pieri, Phys. Rev. E **90**, 043003 (2014).
[31] G. R. Mamatsashvili, V. S. Avsarkisov, G. D. Chagelishvili, R. G. Chanishvili and M. V. Kalashnik, J. Atmos. Sci. **67**, 2972 (2010).
[32] A. Pieri, C. Cambon, F. S. Godeferd, and A. Salhi, Phys. Fluids **24**, 076603 (2012).